Non-invasive neuromagnetic single-trial analysis of human neocortical population spikes

–

Supplementary Material

Gunnar Waterstraat [*1†], Rainer Körber[2†], Jan-Hendrik Storm[2], and Gabriel Curio[1,3]

[1]Charité – Universitätsmedizin Berlin, corporate member of Freie Universität Berlin and Humboldt-Universität zu Berlin, Neurophysics Group, Department of Neurology. Campus Benjamin Franklin. Hindenburgdamm 30, 12203 Berlin, Germany.
[2]Physikalisch-Technische Bundesanstalt (PTB), Department of Biosignals, Abbestraße 2-12, 10587 Berlin, Germany
[3]Bernstein Center for Computational Neuroscience, Philippstr. 13, Haus 6, 10115 Berlin, Germany

January 2021

Contents

*Corresponding Author: gunnar.waterstraat@charite.de
†These authors contributed to this study equally.

1 Supplementary Methods

1.1 Analysis of hfSER autocorrelation across trials

For formalized characterization of the observed response variability, the autocorrelation function (acf) of the responses across trials was calculated separately for the instantaneous amplitude and for the phase of the signal. To this end, the instantaneous amplitude and the phase of the band-pass filtered signal (450 Hz–750 Hz) was extracted as the modulus ($|\cdot|$) and argument (arg $(\cdot)$) of the complex-valued analytic signal, obtained by Hilbert transformation ([1]). To increase the robustness against outliers, the instantaneous amplitude was rank-normalized across trials such that the trial with the smallest instantaneous amplitude at time t was given a value of 1 and the trial with the largest instantaneous amplitude at time t was given a value of N. Let the rank-normalized instantaneous amplitude of the signal at time t and in trial i be denoted as $a_i(t)$, and $\hat{a}_i(t)$ is a standardization to zero mean and unit variance such that

$$\hat{a}_i(t) = (a_i(t) - \overline{a}(t))/\sqrt{\sum_{i=1}^{N}(a_i(t) - \overline{a}(t))^2/N}\,,$$

where $\overline{a}(t) = \sum_{i=1}^{N} a_i(t)/N$. The acf of the instantaneous amplitudes across trials was then calculated as:

$$\mathsf{acf}_a(t,\tau) = \frac{\sum_{i=1}^{N-\tau} \hat{a}_i(t)\hat{a}_{i+\tau}(t)}{(N-\tau)}\,.$$

Note, that this algorithmic approach is equivalent to calculating Spearman's rank correlation coefficient between the instantaneous amplitudes of the signal across trials at different lags.

To calculate the autocorrelation of the phases of the evoked MEG responses, the Circular Correlation Coefficient ([2, 3]) was used: Let $\theta_i(t)$ denote the phase of the evoked response at time t and in trial i. $\theta_i(t)$ can be standardized such that $\hat{\theta}_i(t) = \sin(\theta_i(t) - \overline{\theta}(t))/\sqrt{\sum_{i=1}^{N}\sin(\theta_i(t) - \overline{\theta}(t))^2/N}$, where $\overline{\theta}(t) = \arg(\sum_{i=1}^{N} e^{j\cdot\theta_i(t)})$ and j is the imaginary unit with $j^2 = -1$. The acf of the phases across trials was then calculated as:

$$\mathsf{acf}_\theta(t,\tau) = \frac{\sum_{i=1}^{N-\tau} \hat{\theta}_i(t)\hat{\theta}_{i+\tau}(t)}{(N-\tau)}\,.$$

Note that, in contrast to the instantaneous amplitudes, the phases were not rank-normalized since the Circular Correlation Coefficient is inherently more robust to outliers due to the boundedness of the $\sin(\cdot)$-function to the range $[-1, 1]$.

In order to increase the SNR, the acf was smoothed along the temporal axis using a moving average with a boxcar window of 10 ms width. This procedure is valid since, due to band-pass filtering, neighboring samples are not independent anyway. The integrals of the smoothed acf (denoted $\tau_{\mathsf{int},a}(t)$ for the instantaneous amplitudes and $\tau_{\mathsf{int},\theta}(t)$ for the phases), established as a measure of the total autocorrelation between measurements in the analysis of Monte Carlo methods ([4]), were approximated as

$$\tau_{\mathsf{int}}(t) \approx 1 + 2\sum_{\tau=1}^{\tau_{\mathsf{max}}} \mathsf{acf}(t,\tau)$$

with a maximum calculated trial-lag $\tau_{\mathsf{max}} = 51$.

Significance testing of the autocorrelation integrals was done by standardizing to zero mean and unit variance (across time) and permutation testing against the autocorrelation integrals obtained from 1000 permutations of the data with randomized trial-ordering (with smoothing done in every permutation as described above). The FWER was controlled by a bootstrap procedure ([5]).

To quantify the persistence of the demonstrated autocorrelation across trials, the partial autocorrelation function (pacf) of phases was calculated from the phase-acf (after the described temporal smoothing step) using the Levinson-Durbin recursion method ([6]). In contrast to standard autocorrelation, partial autocorrelation coefficients are controlled for the effect of intermediate lags and can therefore truthfully measure the effect between lagged samples. In order to increase the SNR further, the pacf was subsequently smoothed along the lag-axis using a moving average with a 10-lags-wide boxcar window. Significance testing was done against partial autocorrelation values from

1000 permutations of the data (with smoothing done in the same way as described above) and confined to those temporal intervals with a significant integral of the autocorrelation (i.e., $p < 0.05$). Accordingly, this statistical step is not fully independent from the preceding test of an above-chance autocorrelation integral. The target of this analysis, however, was to identify *which lags* drive a potentially present dependence of the phases across trials. Conservative FWER-controlled p values—indicating the significance of the partial autocorrelation at a specific lag given the selected interval—were obtained by the same bootstrap procedure as above ([5]).

1.2 Re-Analysis of previous MEG data

1.2.1 MEG equipment

For this study, data from [7] has been re-analyzed. In that study, a predecessor of the novel low-noise MEG system had been used. The system consisted of in total 18 magnetometers, arranged in two levels separated by a baseline of 90 mm. At the bottom level, 6+1 circular pick-up coils (for the z-direction of the magnetic flux) were aranged in a hexagonal shape, each with a diameter $d = 17.1$ mm and at a centre-to-centre distance of 30 mm. A reference magnetometer at the second level, 90 mm above, allowed to set up an axial gradiometer setting. All sensors were SQUID-based and customly constructed according to a previously published scheme [8]. The module was operated in a low-noise liquid helium dewar (Fujihira Co., Ltd, Tsukuba, Japan) with a flat bottom ($d = 250$ mm) and an estimated warm-cold distance of 28 mm at a temperature of 4.2 K (24 mm at room temperature). All recordings were performed in the shielded room *BMSR-2* of the Physikalisch-Technische Bundesanstalt.

Accordingly, the system used in [7] differs in two instrumental points from the novel low-noise MEG system used in this study ([9]):

- The construction of a custom dewar (Low Intrinsic NOise Dewar 2; 'LINOD2') with a shorter warm-cold distance of only 12.9 mm (at 4.2 K) for the novel low-noise MEG system allowed to reduce the distance between the head surface and the bottom pick-up coil. Hereby, neuronal magnetic fields—with a flux density decaying proportional to the squared distance between source and sensor—are captured at a stronger field strength.
- While, with a white noise spectral density of 1.28 fT$/\sqrt{\text{Hz}}$, the system in [7] is superior to commercially available systems, the novel system design used in this study reduced the system noise by even another order of magnitude to 0.18 fT$/\sqrt{\text{Hz}}$.

Both points—increased signal strength and decreased system noise—directly lead to an increase of the signal-to-noise ratio (SNR) of the MEG and enabled single-trial analysis of hfSERs in the first place.

1.2.2 MEG recordings and analysis

In [7], hfSERs were elicited in three subjects by electric stimulation of the right median nerve at a repetition rate of $9/\text{s}$. Subjects 1 and 2 of that study coincide with subjects S3 and S4 of the present study and allowed a direct comparison. Nerve stimuli of 200 µs duration were applied above motor threshold and the sensor array was placed above the left hemisphere of the head with the central sensor tangentially above the midpoint between C3 and T3. For a fair comparison to the novel data, we selected the first 2500 trials from a total of $N = 16200$ repetitions. Out of the 6 sensors in the bottom level, referenced to the sensor in the second level, the montage with the highest peak-to-peak amplitude of hfSERs was chosen for further analysis. All the subsequent analyses were done analogously to the newly acquired data of this study.

1.2.3 Results

In the re-analysis of data from [7], *phase-locked* hfSERs could be observed only in two of three subjects. Critically, phase-insensitive hfSER contributions at 600 Hz and evidence of amplitude variability of hfSER responses at the single-trial level were not detectable in any of these three subjects. Note that this is not attributable to the individual hfSER strength, since two subjects participated in both studies (S3 and S4 of the present study). This SNR-dependent non-detectability of phase-insensitive hfSER components is in agreement with computational modeling [10].

As a consequence of the low SNNR, no correlation was found between the amplitudes of hfSER responses and the concomitant low-frequency response ('N20m'). Analysing the relation between latencies of the low-frequency and the burst response yielded no significant results in all but the one measurement with the weakest burst response

and lowest SNR (subject S4), a finding well explainable by the inflation of p values by multiple testing. Matching the non-detection of phase-insensitive hfSER activity and hfSER variability in the re-analyzed MEG data from [7], obtained at a lower SNR, analysis of autocorrelation between single-trial hfSER responses conducted in these data revealed negative results altogether.

Result figures from the recordings are available together with the analysis code at `www.github.com/neurophysics/2021-hfMEG`.

References

[1] Le Van Quyen M et al. (2001) Comparison of Hilbert transform and wavelet methods for the analysis of neuronal synchrony. *J. Neurosci. Methods* 111(2):83–98.

[2] Fisher NI, Lee AJ (1983) A correlation coefficient for circular data. *Biometrika* 70(2):327–332.

[3] Burgess AP (2013) On the interpretation of synchronization in EEG hyperscanning studies: a cautionary note. *Front. Hum. Neurosci.* 7:881.

[4] Sokal A (1997) Monte carlo methods in statistical mechanics: Foundations and new algorithms in *Functional Integration: Basics and Applications*, eds. DeWitt-Morette C, Cartier P, Folacci A. (Springer US, Boston, MA), pp. 131–192.

[5] Romano JP, Wolf M (2016) Efficient computation of adjusted p-values for resampling-based stepdown multiple testing. *Stat. Probab. Lett.* 113:38–40.

[6] Durbin J (1960) The fitting of Time-Series models. *Revue de l'Institut International de Statistique / Review of the International Statistical Institute* 28(3):233–244.

[7] Storm JH, Drung D, Burghoff M, Körber R (2016) A modular, extendible and field-tolerant multichannel vector magnetometer based on current sensor SQUIDs. *Superconductor Science and Technology* 29(9):094001.

[8] Drung D et al. (2007) Highly sensitive and Easy-to-Use SQUID sensors. *IEEE Trans. Appl. Supercond.* 17(2):699–704.

[9] Storm JH, Hömmen P, Drung D, Körber R (2017) An ultra-sensitive and wideband magnetometer based on a superconducting quantum interference device. *Appl. Phys. Lett.* 110(7):072603.

[10] Waterstraat G et al. (2012) Are high-frequency (600 hz) oscillations in human somatosensory evoked potentials due to phase-resetting phenomena? *Clin. Neurophysiol.* 123(10):2064–2073.

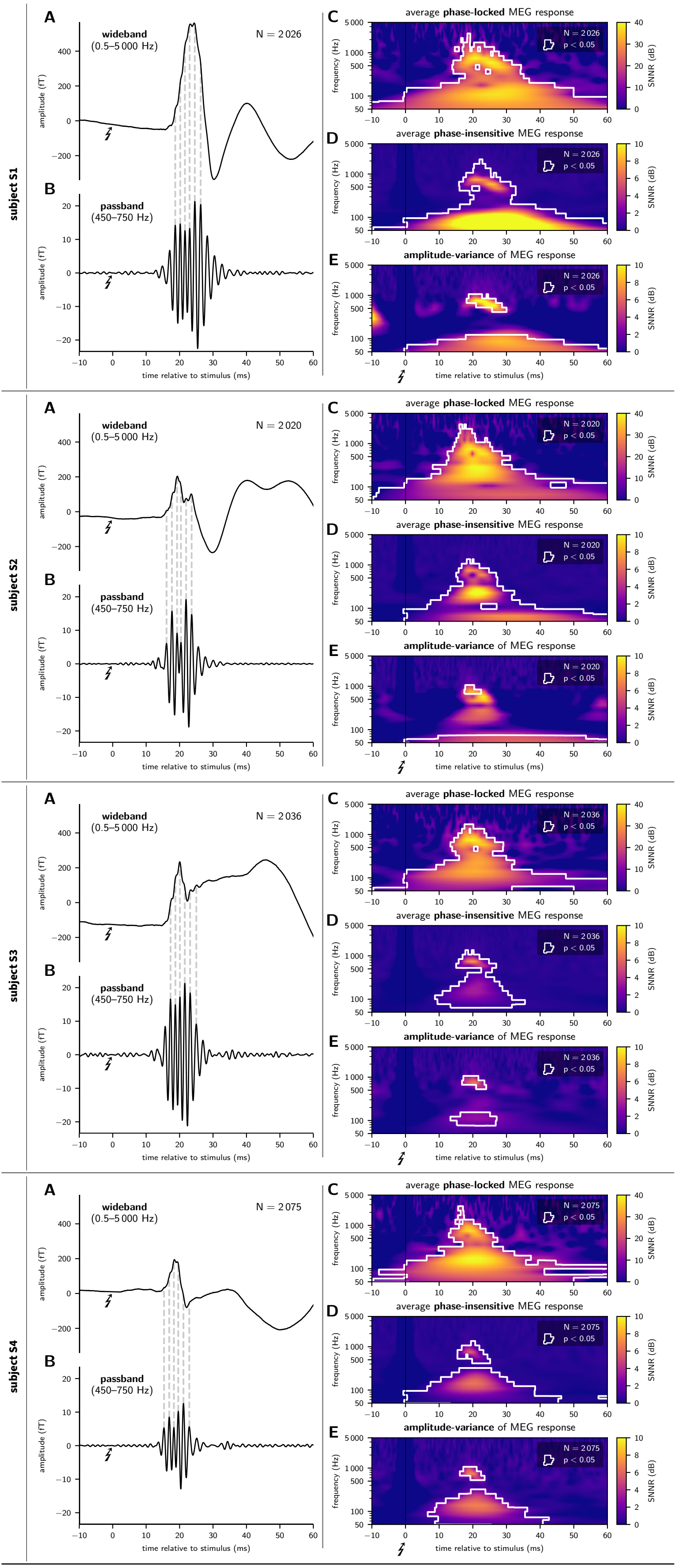

Figure A2: Averaged evoked responses **(A + B)** and time-frequency (tf) transformed responses **(C + D + E)** after median nerve stimulation for all four subjects. The individual images and their structure correspond to Figure 2 of the main article and are described in detail there. Subjects are presented in descending order according to the single-trial signal-to-noise ratio of the hfSER. **A:** wideband response with the first cortical response at around 20 ms (N20m) as main response. **B:** averaged hfSER isolated by band-pass filtering in the 450–750 Hz passband. Single peaks of the hfSER responses can be delineated as humps and notches on the wideband response. Panel **C** shows the tf transformation of the averaged response which is sensitive solely to at least partially phase-locked components of the response. Panel **D** shows the average of the tf-transformed single-trial amplitudes and is therefore phase-insensitive. Hence, both images depict complementary properties of the responses. Panel **E** indicates the presence of single-trial amplitude variability exceeding noise variability. The methodology to create the tf transforms and their interpretation are descibed in detail in the main article. Values in every tf tile were normalized as ´signal-plus-noise'-to-noise ratio (SNNR) by division through frequency-specific mean values obtained in a pre-stimulus segment.

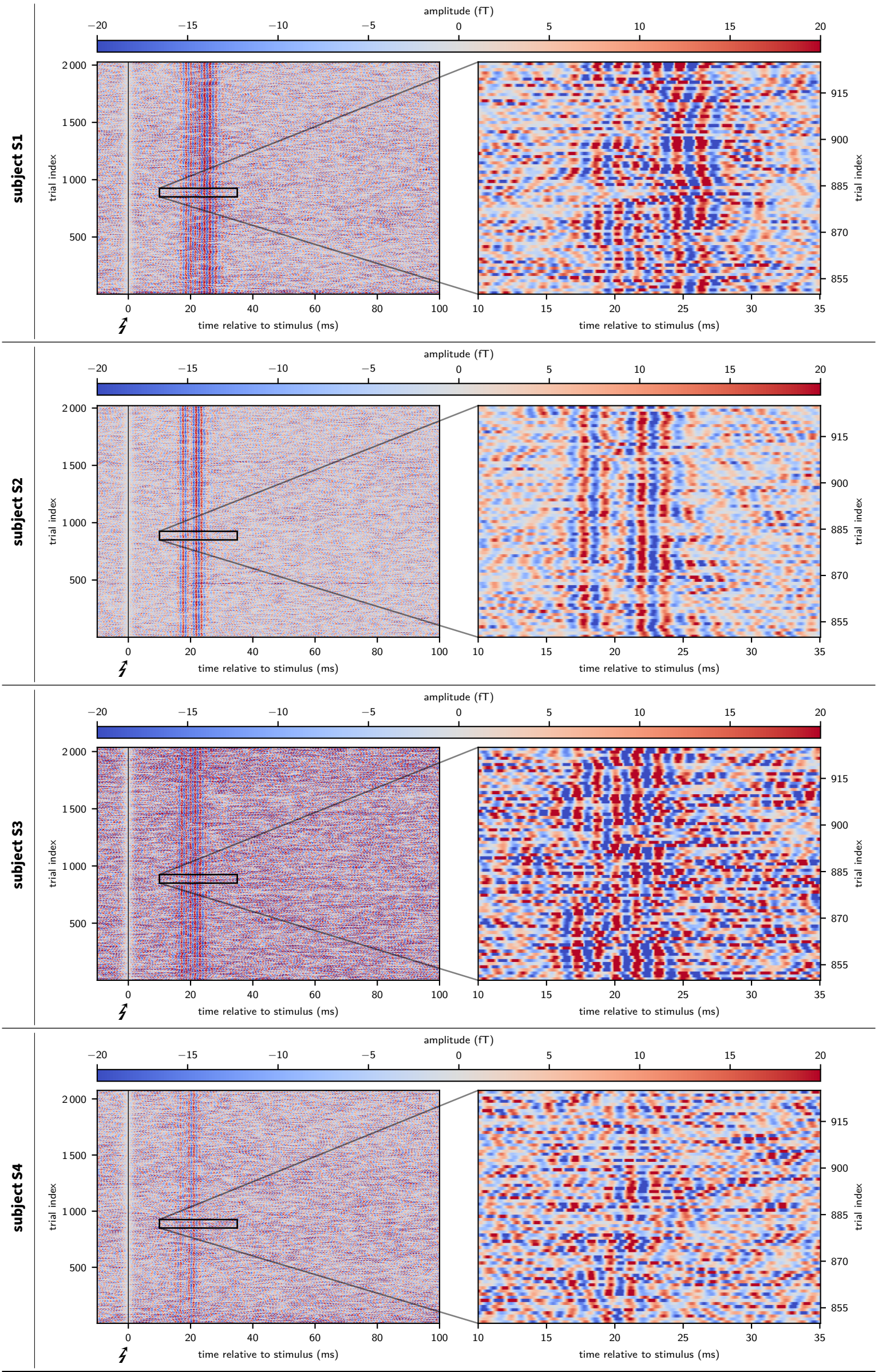

Figure A3: Single-trial hfSER with amplitudes coded as color saturation. The image and its structure corresponds to Figure 3 in the main article. Single-trial hfSERs show large variability with reduced or missing first half of the response while the second half remains present and vice versa. Additionally, slow fluctuations of the latency of the responses can be observed. Further, the identical scaling of the amplitude-to-color code across all four subjects allows to discriminate the influence of signal and noise level in the four subjects. For example, subject S1 has the strongest hfSERs; however, the noise level in subject S2 is lower. Subject S3 partially outweighs its strong noise level by strong hfSERs. Finally, the hfSER is weakest in subject S4.

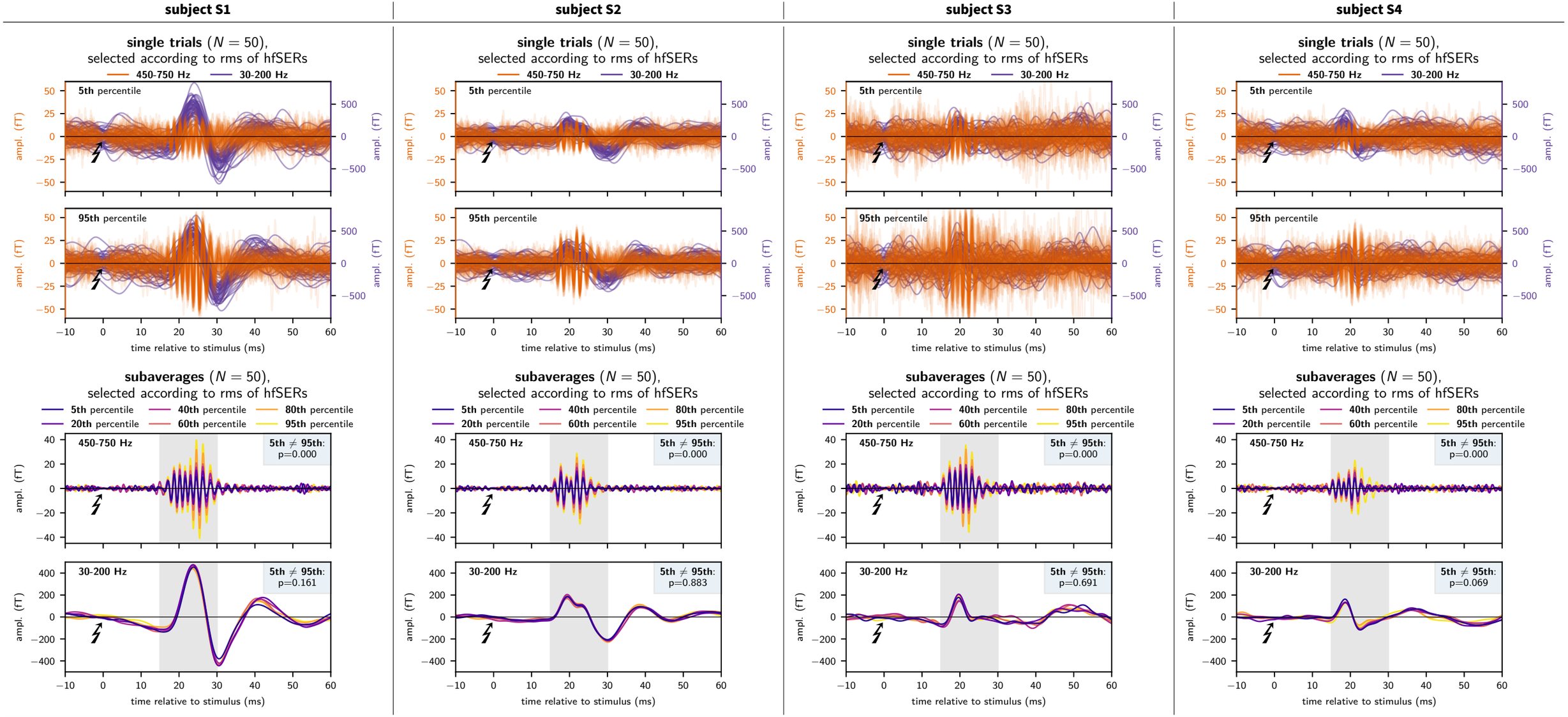

Figure A4: Analysis of single trials and subaverages of $N = 50$ trials, selected according to the rms of the hfSER for all subjects. The methodology to create the figure and its structure are descibed in detail in Figure 4 in the main article. Low-frequency responses were not significantly different between the 5th and 95th percentile of trials selected according to the hfSER amplitude.

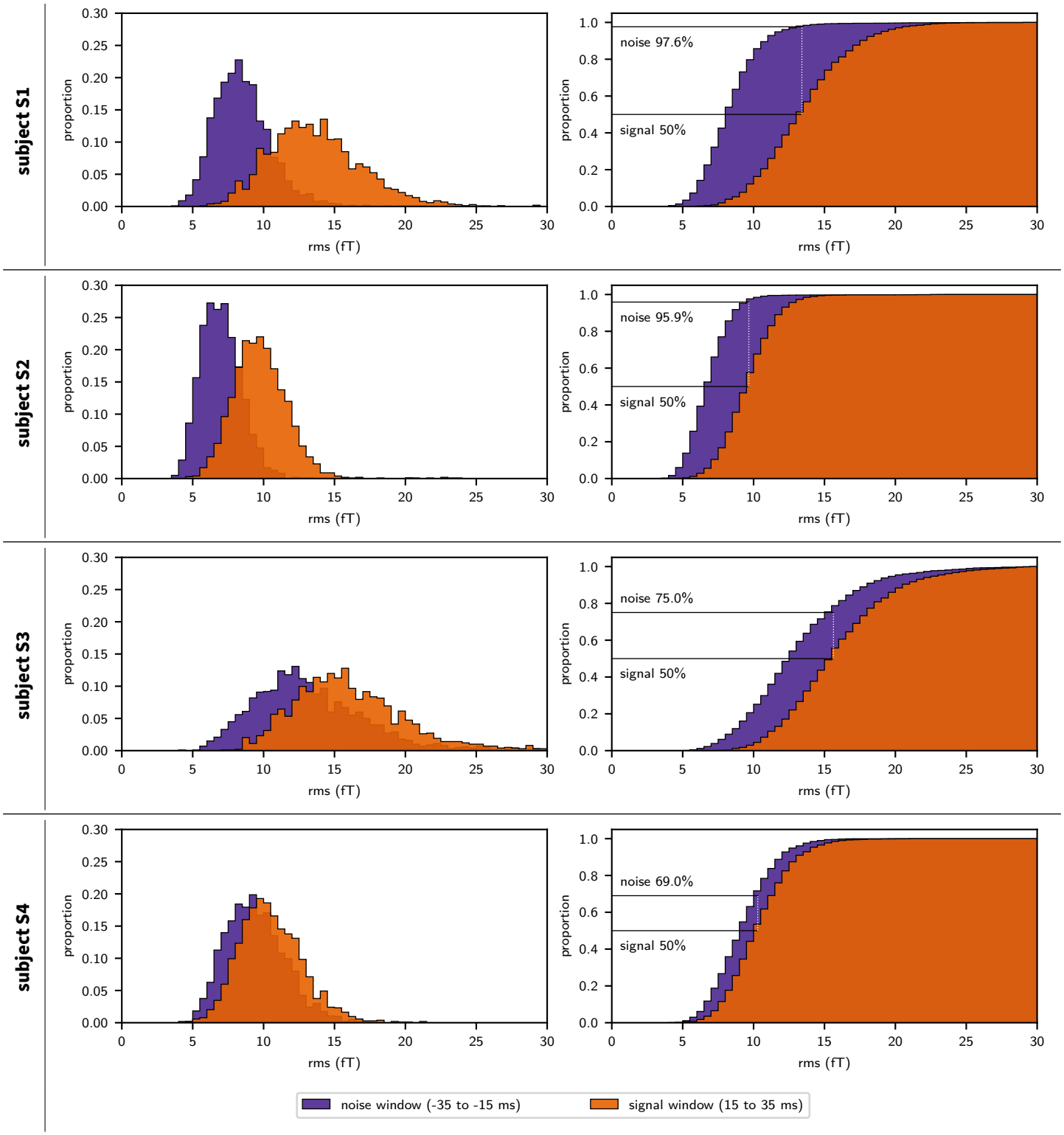

Figure S1: Distribution (**left**) and cumulative distribution (**right**) of single-trial rms amplitudes in a noise window (-35 to -15 ms) and in a signal window ($+15$ to $+35$ ms) after band-pass filtering ($450 - 750$ Hz). For all measurements with the novel low-noise MEG system, the distribution of amplitudes in the burst window is shifted to the right due to additive hfSER activity. The SNR is reflected in the extent of this 'shift' and the variance of the distributions. In the two subjects with the highest SNR, the upper 50 % of burst amplitudes share only minimal overlap with the distribution of noise amplitudes (<5 %), allowing for a reliable differention of single-trial response strength variability.

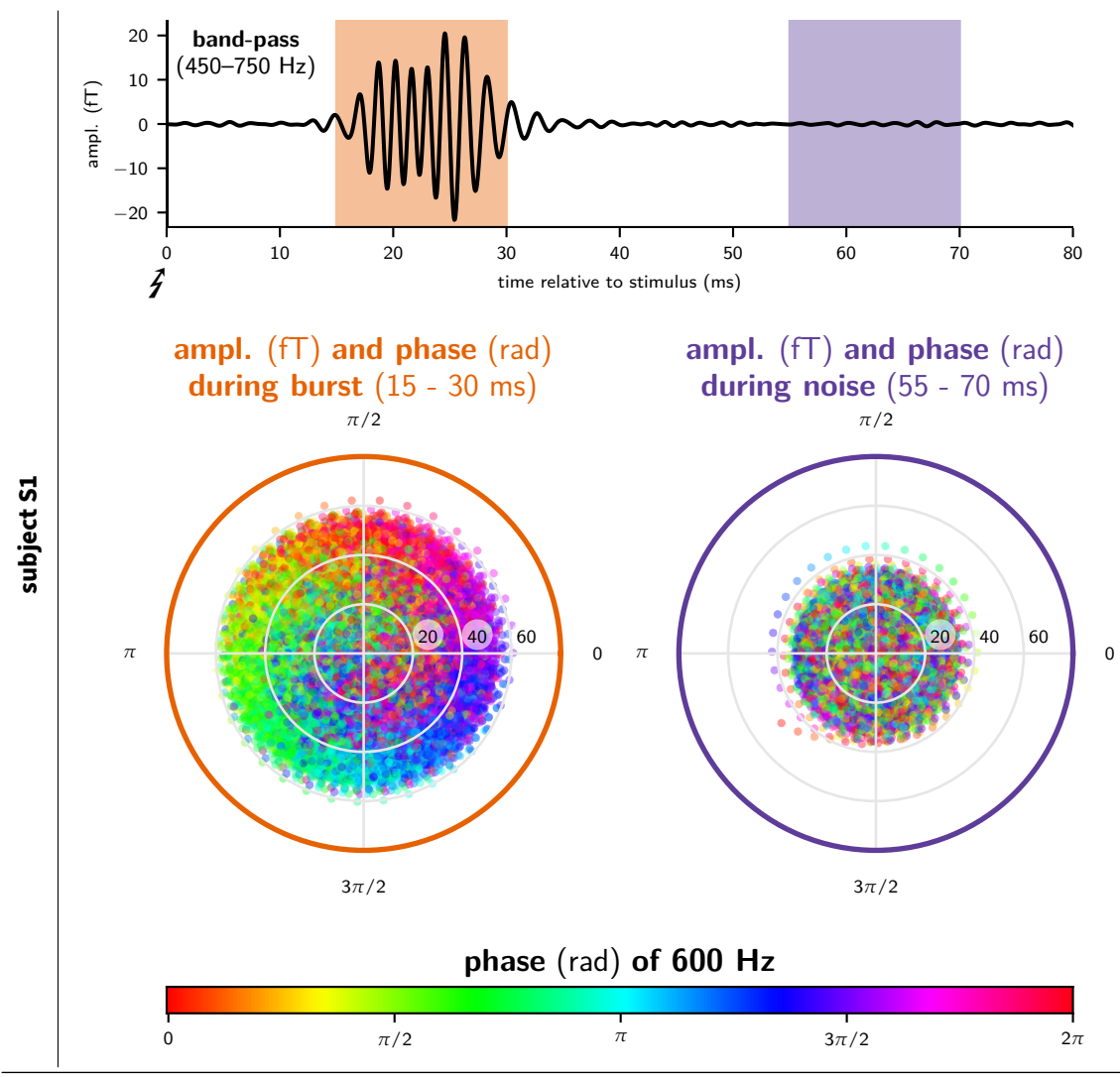

Figure S2: Comparison of instantaneous single-trial amplitudes and phases between burst window ($15 - 30$ ms; **left**) and noise window ($55 - 70$ ms; **right**) and phase alignment to a constant 600 Hz oscillation. The average hfSER after band-pass filtering ($450 - 750$ Hz; **top**) is shown as reference for the placement of the windows. On polar plots (**bottom**), the instantaneous phase and amplitude of a signal at a single timepoint (obtained by Hilbert transformation) is represented by a point at a certain angle (in rad) and distance (in fT) from the origin of the plot. Here, colour additionally represents the phase of a corresponding sine wave at a constant frequency of 600 Hz with $t_0 = 15/55$ ms. In the noise window, the alignment of phases to a 600 Hz oscillation is random. In contrast, for recordings with the novel low-noise MEG system, the phases during the burst window are locked to a 600 Hz oscillation as represented by the rainbow-like color ordering across the angles of the polar plots. Additionally, single-trial amplitudes are increased during the burst window as shown by larger distances from the origin, with the 'signal-plus-noise'-to-noise ratio (SNNR) given by the ratio of the radii of the point clouds between the two windows.

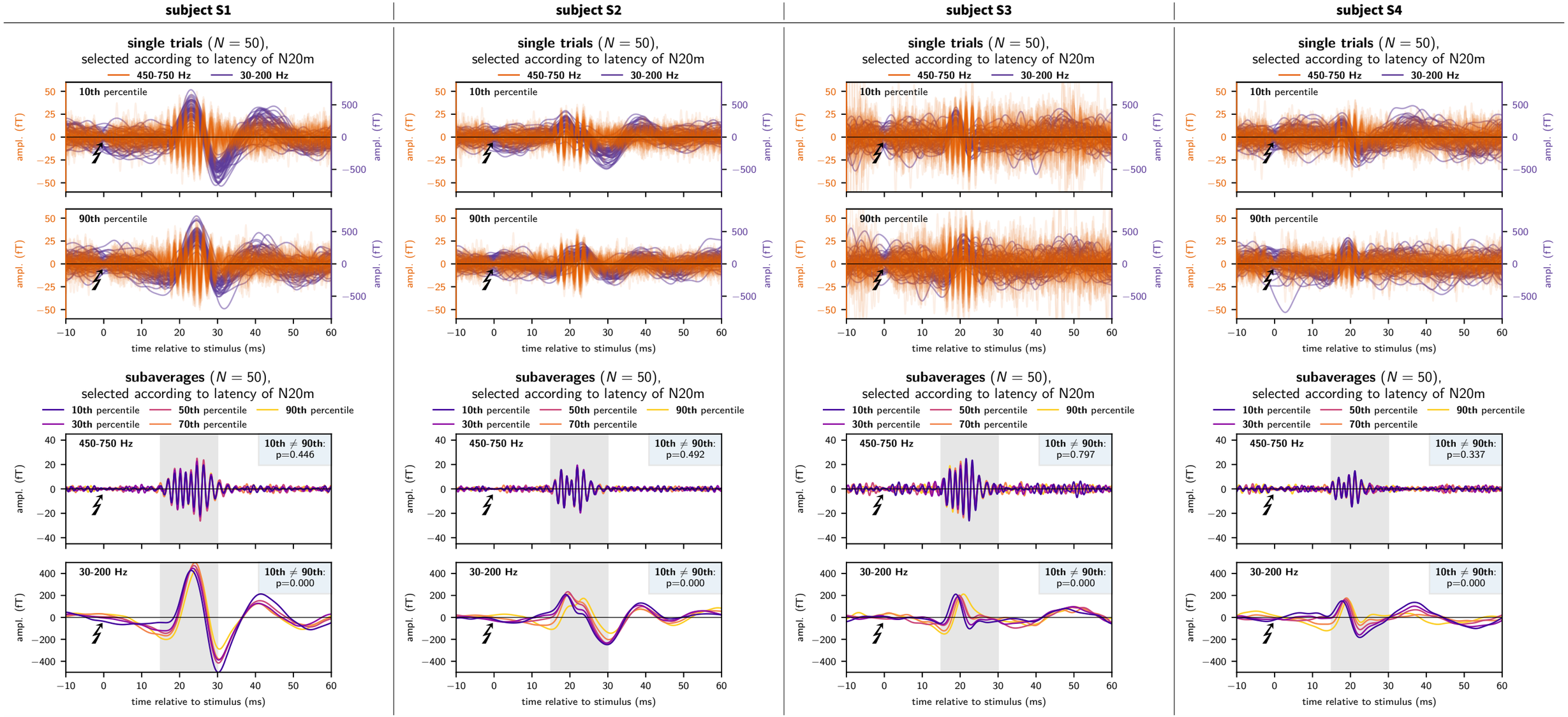

Figure S3: Analysis of single trials and subaverages of $N = 50$ trials, selected according to the *latency* of the low-frequency N20m response for all subjects. The methodology to create the figure and its structure are analogous to Figure 4 in the main article (except for sorting now according to the *latency* of the N20m instead of hfSER amplitude). High-frequency responses were not significantly different between the 5th and 95th percentile of trials selected according to the N20m latency despite successful selection of trials with early and late responses.

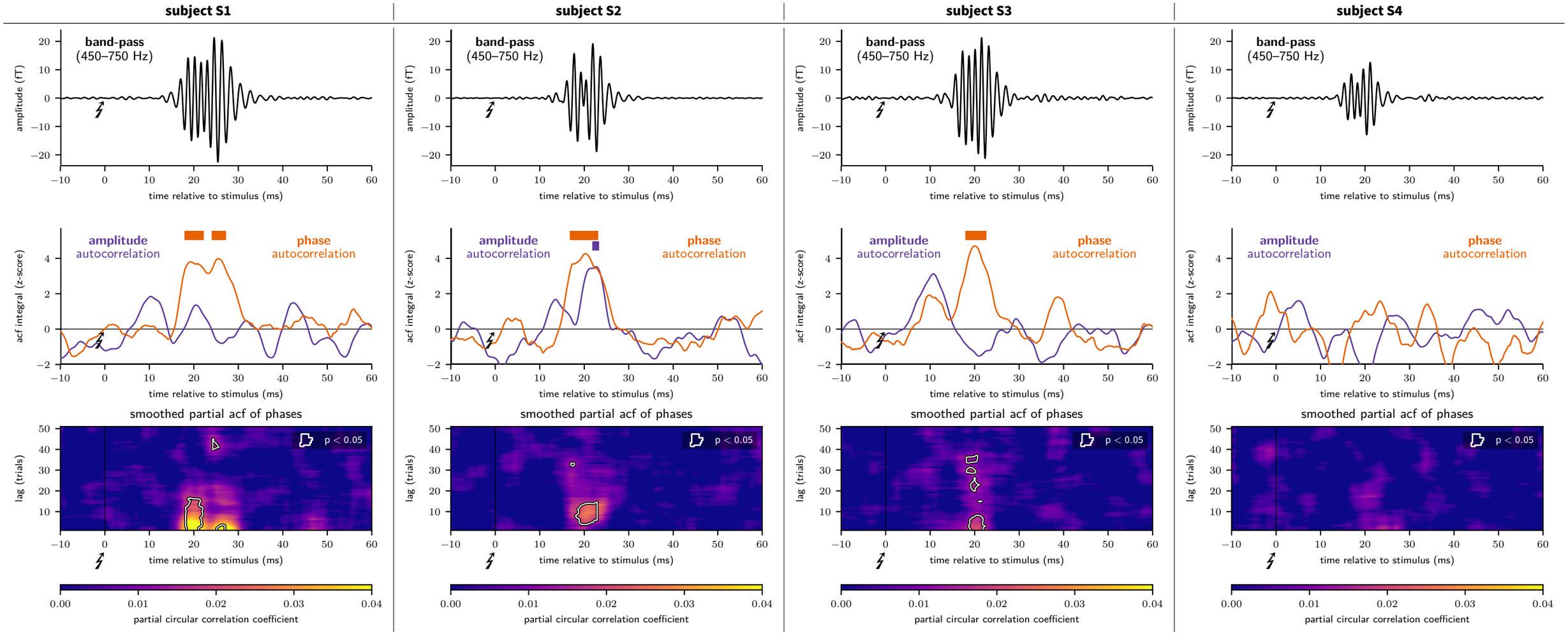

Figure S4: Analysis of the autocorrelation function (acf) *across trials* done for all four subjects. The averaged band-pass filtered hfSER is shown as a temporal reference (**top panel**). The autocorrelation of hfSERs across trials was condensed to the integral of the acf (**middle panel**) and standardized to zero mean and unit variance (z-score). The analysis was performed independently for the instantaneous amplitude (**blue curve**) and the phase (**orange curve**) of hfSERs. Significant segments are marked as bars of corresponding color above the curves. For the novel low-noise MEG system, a significant increase of autocorrelation was obtained for the phase signal in three of four subjects (the fourth subject had the lowest phase-insensitive single-trial SNNR). Partial autocorrelation of phases (**bottom panel**) shows a significant correlation up to a maximum lag of 40 trials (p values were FWER-corrected). Thus, at a stimulation rate of 3.27 /s, phases of single-trial responses are correlated for more than 10 seconds. Subject S2 had significant autocorrelation of signal amplitudes during the hfSER period. This finding will be addressed in more detail in future studies.